This article has been accepted for publication in IEEE Geoscience and Remote Sensing Letters. This is the author's version which has not been fully edited and content may change prior to final publication. Citation information: DOI 10.1109/LGRS.2024.3379196

SNRI: A Signed Normalized Range Index for Remote Sensing of Panax Notoginseng Plantations

Xiangjian Xie, Alim Samat, *Member, IEEE,* Yufeng He, Yuhong Jiang

***Abstract*—Panax Notoginseng is a widely recognized medicinal herb in Chinese traditional medicine. Investigating the cultivation of P. notoginseng is crucial for ecological preservation and effective land management. In our study, we conducted an analysis of the spectral properties of P. notoginseng plantations along with various other land cover types. As a result, we have introduced a novel index called the Signed Normalized Range Index (SNRI), based on the maximum and minimum reflectance values across all bands of the multispectral imagery. Through experiments conducted on Landsat-8 OLI images obtained from Yunnan, China, we performed quantitative assessments of separability measurements. SNRI has shown great potential in enhancing the identification of P. notoginseng, with an average Jeffries-Matusita separability of 1.378 compared to other land covers. Furthermore, we conducted a comparative analysis of the SVM classification results using several spectral indices for dark target extraction. The comparison affirmed the superior performance of SNRI in accurately distinguishing P. notoginseng plantations from other land cover types. It is promising to explore the application of SNRI in remote sensing estimation and change monitoring of the P. notoginseng planting area, as well as other land covers with similar lower reflectance ranges.**

***Index Terms*—Panax notoginseng, SNRI, Landsat-8 OLI, remote sensing, spectral index**

I. Introduction

Panax Notoginseng holds a prominent position in the Chinese materia medica as a highly regarded medicinal herb. Its use as a hemostatic agent gained significant recognition among the Chinese military by the 1890s, and the root of P. notoginseng was highly valued [1]. It has been assigned various names in botanical and medical literature, including *Aralia Bipinnatifida* [2], Panax ginseng [3], and also Sanqi [4], which refers to the plant's three to four whorled leaves, each bearing seven leaflets, resembling Panax pseudo-ginseng Wall. P. notoginseng predominantly thrives in the mixed forests of high mountains in Southwest China, ranging from 1,000 to 3,000 meters above sea level, along the Tropic of Cancer. Currently, wild varieties of P. notoginseng are scarce, with most cultivation occurring artificially. Commercial products primarily originate from cultivation in the mountainous regions of Yunnan Province. Plantations are typically established on slopes at altitudes of 800 to 1,000 meters [5]. The extensive usage of P. notoginseng throughout China, coupled with its substantial export volume, has led to a significant increase in cultivation area over the past decade. However, this rapid expansion of P. notoginseng cultivation has resulted in a rapid transformation of land cover, potentially exerting considerable pressure on the local ecosystem [6]. Therefore, investigating P. notoginseng plantations is imperative for both ecological conservation and effective land use management.

Panax notoginseng is a shade-loving plant commonly grown under black sheds made of shading nets to protect it from direct sunlight. These sheds provide shading for the plant throughout its 2-3 year lifecycle, with a light transmittance of 8-20%. This unique shading characteristic is important for detecting P. notoginseng from remote sensing images. [7]. In recent years, researchers have explored methods to improve the mapping of P. notoginseng plantations using remotely sensed imagery. The use of high-resolution satellite images has gained interest in P. notoginseng plantation mapping [8]. However, the high cost and limited accessibility pose challenges, current research using medium-resolution image data often employs sample-supervised training methods for classification [9], [10]. Although these methods achieve high detection accuracy, their complex algorithms often limit their practical application due to computational efficiency and robustness issues. Therefore, there is a need to develop a simple and generalizable model.

Spectral indices help in modeling, predicting, or inferring surface processes, which have apparent advantages due to their easy implementation and convenience in practical applications [11]–[16]. In this paper, we propose the use of a spectral index derived from Landsat satellite data to enhance

Manuscript received on 29-Dec-2023; revised on 04-Mar-2024; accepted on 14-Mar-2024. This work was supported in part by the Science and Technology Research Fund of Education Department of Jiangxi Province under Grant GJJ2200743 and in part by the National Natural Science Foundation of China under Grant 42301533. (Corresponding author: Yufeng He, Xiangjian Xie)

Xiangjian Xie and Yuhong Jiang are all with the Key Laboratory of Mine Environmental Monitoring and Improving around Poyang Lake of Ministry of Natural Resources, and with the School of surveying and Geoinformation Engineering, East China University of Technology, Nanchang, 330013, China (e-mail: xiexj@ecut.edu.cn; jiangyuhong0509@gmail.com).

Alim Samat is with the State Key Laboratory of Desert and Oasis Ecology, Xinjiang Institute of Ecology and Geography, CAS, Urumqi 830011, China (e-mail: alim_smt@ms.xjb.ac.cn).

Yufeng He is with the Key Laboratory of Poyang Lake Wetland and Watershed Research, Ministry of Education, Jiangxi Normal University, Nanchang 330022, China (e-mail: Yuf.he@jxnu.edu.cn).

Authorized licensed use limited to: Xian Jiaotong University. Downloaded on March 20,2024 at 23:26:41 UTC from IEEE Xplore. Restrictions apply.
© 2024 IEEE. Personal use is permitted, but republication/redistribution requires IEEE permission. See https://www.ieee.org/publications/rights/index.html for more information.

This article has been accepted for publication in IEEE Geoscience and Remote Sensing Letters. This is the author's version which has not been fully edited and content may change prior to final publication. Citation information: DOI 10.1109/LGRS.2024.3379196

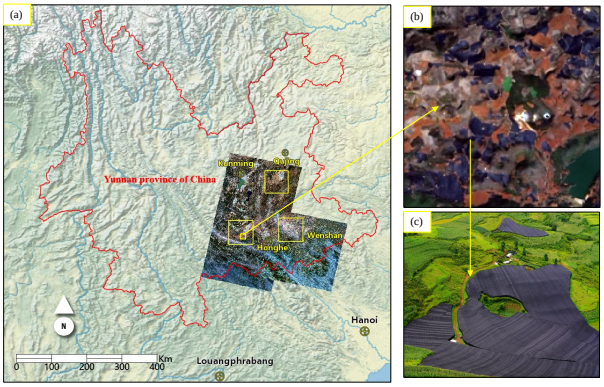

Fig. 1: Study areas, (a) geographical location map and Landsat-8 OLI images of three study areas in Yunnan province, China. (b) Scene of the true color composite image (R:4, G:3, B:2). (c) Field photo of P. notoginseng plantations with black sheds.

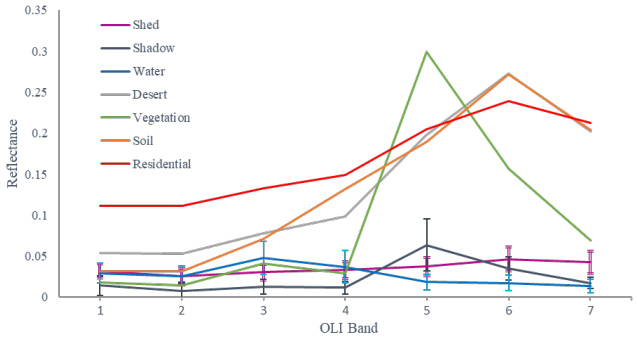

Fig. 2: Reflectance spectra of the main biophysical compositions of the surface in study areas.

the mapping of P. notoginseng plantations. Our objectives are to develop a spectral index for P. notoginseng plantation mapping and to assess the performance of the derived index in accurately distinguishing P. notoginseng plantations from other land cover types. This assessment will involve the comparison of class separability measurements and cross-validation classification accuracy.

The remainder of this paper is organized as follows. Section II provides a description of the study areas and datasets used. Section III presents the proposed spectral index. Section IV illustrates the experimental results obtained. Conclusion are drawn in Section V at last.

II. Study Areas and Datasets

The study focused on three square study areas located in Wenshan Prefecture, Honghe Prefecture, and Qujing in Yunnan Province, China. These areas were selected to represent the expansion of Panax notoginseng cultivation from its origin in Wenshan Prefecture (as shown in Fig.1). The main biophysical compositions of the surface in these areas include green vegetation, soil, water, residential areas, bare bedrock, and P. notoginseng sheds. The dominant land cover types consist of forests, cultivated land, deserts, and residential areas, with open waters and P. notoginseng plantations as secondary land cover types. For this study, three Landsat-8 Operational Land Imager (OLI) images (path 128-129, row 43-44) were used. These images were acquired between 2015 and 2018, covering the study areas. The Landsat 8 Collection 2 Surface Reflectance product was employed, which underwent topographic, geometric, and radiometric corrections [17].

III. Methodology

The methodology for constructing the spectral index for P. notoginseng plantation mapping using Landsat-8 OLI imagery can be summarized as follows:

1) Analysis of the spectral reflectance characteristics of P. notoginseng plantations in comparison to other land cover types.
2) Proposal of a Signed Normalized Range Index (SNRI) and comparison with commonly used spectral indices for remote sensing of dark targets.
3) Performance assessment of mapping P. notoginseng plantations using the proposed index and other relevant indices.

A. Analyzing the spectral reflectance characteristics

In the analysis, the reflectance spectra of various land cover types were studied. Utilizing high-resolution images from Google Earth, a total of 5649 land cover samples were selected to calculate the average reflectance of seven representative land cover types in the study areas. Fig.2 shows the mean reflectance of typical surface objects.

The analysis revealed that major land cover types like vegetation, residential areas, and desert land have a maximum reflectance in the near-infrared (NIR) or shortwave infrared 1 (SWIR1) band and a minimum reflectance in Band 1 or Band 2. The reflectance ranges for these land cover types were relatively large, above 0.19 (Table I). In contrast, the reflectance of P. notoginseng shed samples had a maximum in the SWIR1 band, but their reflectance ranges were smaller, averaging 0.024. Shadow and open water samples also had relatively small reflectance ranges. Mountain shadow samples had a higher range due to the presence of vegetation, averaging 0.049. Open water samples had an average reflectance range of 0.037, similar to the sheds. Importantly, the reflectance characteristics of water bodies differed from other land cover types, with a maximum reflectance in the visible region and a minimum reflectance in the infrared region. This distinction allows for the enhancement of P. notoginseng shed signals while suppressing signals from other land cover types like water, vegetation, and bare land, based on the reflectance range and extreme band positions of Landsat 8 OLI images.

Authorized licensed use limited to: Xian Jiaotong University. Downloaded on March 20,2024 at 23:26:41 UTC from IEEE Xplore. Restrictions apply.
© 2024 IEEE. Personal use is permitted, but republication/redistribution requires IEEE permission. See https://www.ieee.org/publications/rights/index.html for more information.

This article has been accepted for publication in IEEE Geoscience and Remote Sensing Letters. This is the author's version which has not been fully edited and content may change prior to final publication. Citation information: DOI 10.1109/LGRS.2024.3379196

TABLE I: The maximum and minimum spectral reflectance values, band positions, and range of spectral reflectance observed in typical land-cover samples within the study areas.

Land-cover	Min	Max	Range	Min Band	Max Band
Vegetation	0.018	0.249	0.231	0.443	0.865
Water	0.015	0.052	0.037	2.201	0.561
Soil	0.033	0.283	0.250	0.443	1.609
Desert	0.051	0.242	0.191	0.443	1.609
Residential	0.099	0.336	0.237	0.443	1.609
Shadow	0.015	0.064	0.049	0.482	0.886
Shed	0.035	0.058	0.024	0.443	1.609

TABLE II: Spectral indies formulas and corresponding references.

Index	Formulas	Source
NDWI	$(\rho_{B_3} - \rho_{B_5})/(\rho_{B_5} + \rho_{B_3})$	[12]
MNDWI	$(\rho_{B_3} - \rho_{B_6})/(\rho_{B_6} + \rho_{B_3})$	[13]
AWEI$_{sh}$	$\rho_{B_1} + 2.5\rho_{B_2} - 1.5(\rho_{B_4} + \rho_{B_5}) - 0.25\rho_{B_7}$	[14]
AWEI$_{nsh}$	$4(\rho_{B_2} - \rho_{B_5}) - 2.5\rho_{B_4} + 2.75\rho_{B_7}$	[14]
MBWI	$2\rho_{B_3} - \rho_{B_4} - \rho_{B_5} - \rho_{B_6} - \rho_{B_7}$	[15]
CSI	$(\rho_{B_5} + \rho_{B_6})/2$	[16]
NDPI	$(\rho_{B_2} - \rho_{B_3})/(\rho_{B_2} + \rho_{B_3})$	[8]
Max	$Max(\rho_{B_{1-7}})$	This work
Min	$Min(\rho_{B_{1-7}})$	This work
NDRI	(Max-Min)/(Max+Min)	This work
SNRI	$(\rho_{B_5} - \rho_{B_3})/\lvert\rho_{B_5} - \rho_{B_3}\rvert$*NDRI	This work

B. The construction of SNRI

Index-based methods are commonly used to highlight the difference between specific land cover types and the background in multispectral imagery. These methods compute a normalized difference between spectral bands where the land covers exhibit their highest and lowest reflectance values [11]–[13]. For example, the Normalized Difference Panax Notoginseng Index (NDPI) has been proposed to discriminate between P. notoginseng and water bodies [8]. Table II provides examples of widely used correlation spectral index expressions and their references.

Based on the spectral reflectance characteristics of land cover types (specifically, the smaller reflectance range of P. notoginseng sheds compared to other land cover types), we propose a SNRI to enhance the intensity contrast between P. notoginseng sheds and the background. The SNRI is defined as follows:

$$SNRI = S * \frac{Max(\rho_{B_{1-7}}) - Min(\rho_{B_{1-7}})}{Max(\rho_{B_{1-7}}) + Max(\rho_{B_{1-7}})} \quad (1)$$

$$S = (\rho_{B_5} - \rho_{B_3})/|\rho_{B_5} - \rho_{B_3}| \quad (2)$$

In the eqs, ρ_{Bi} represents the reflectance of the ith band. Max and Min are the maximum and minimum reflectance values across all bands. S is a sign coefficient used to distinguish between P. notoginseng sheds and open water, defined by the green and infrared bands of the multispectral imagery. Typically, for open water, the reflectance in the green band is greater than that in the infrared band, resulting in a sign coefficient of -1. Conversely, for Panax notoginseng sheds, the reflectance in the infrared band is greater than that in the green band, leading to a value of 1 for the sign coefficient. Therefore, in theory, a positive SNRI value indicates P. notoginseng sheds, while a negative value indicates open water.

C. Performance assessment

To evaluate the effectiveness of SNRI in distinguishing P. notoginseng sheds from other land covers in rural/suburban environments, separability measurements and a confusion matrix were calculated. The spectral discrimination index (SDI) and Jeffries-Matusita (J-M) were used to quantitatively assess the separability between sheds and other land covers [18]–[20]. Higher values of these measurements indicate better separation, while lower values suggest spectral confusion. J-M greater than $\sqrt{1.9}$ indicate very good separability. If the J-M is between $\sqrt{1.7}$ and $\sqrt{1.9}$ then separation is fairly good [19]. For comparative analysis, eleven other spectral indices (NDVI, NDWI, MNDWI, CSI, MBWI, AWEIs, NDPI, Max, Min, and NDRI) were also evaluated for their ability to enhance the signal difference between P. notoginseng sheds and other land covers.

In addition to separability measurements, a Support Vector Machine (SVM) classification approach was employed using the two indices with the best separability as explanatory variables. The SVM classification utilized a radial basis function kernel in ENVI 5.6 software. The classification results were smoothed with a 3x3 majority filter to reduce noise. The accuracy of the classification was assessed using a confusion matrix, and performance metrics such as precision, recall, and F1-score were compared for P. notoginseng plantations.

IV. Experimental results and discussion

In this section, we present experimental results using three Landsat-8 OLI images from Yunnan Province, China. The SNRI was calculated using Using Eq. (1) and visualized in Fig.3. The SNRI analysis revealed that open waters had the lowest values, followed by sheds, while residential, rocky desertification, shadow and bare soil patches had medium values, and vegetated areas had the highest SNRI values. In addition to visual examination, quantitative analyses using SDI and J-M separability measurements were conducted. The J-M (see Table III) were greater than 1.413 for shed-desert, shed-water, shed-soil, and shed-vegetation pairs, indicating good separability between P. notoginseng sheds and these land covers. However, the separability between sheds and residential was not satisfactory, with a J-M of slightly less than $\sqrt{1.7}$. This reduced separability was due to smaller reflectance ranges in some residential samples. Additionally, the presence of architectural samples in shadows further decreases the separability with the plantations.

SNRI outperformed other indices such as NDWI and MNDWI in distinguishing sheds from open waters, with

Authorized licensed use limited to: Xian Jiaotong University. Downloaded on March 20,2024 at 23:26:41 UTC from IEEE Xplore. Restrictions apply.
© 2024 IEEE. Personal use is permitted, but republication/redistribution requires IEEE permission. See https://www.ieee.org/publications/rights/index.html for more information.

This article has been accepted for publication in IEEE Geoscience and Remote Sensing Letters. This is the author's version which has not been fully edited and content may change prior to final publication. Citation information: DOI 10.1109/LGRS.2024.3379196

TABLE III: SDI and J-M values between P. notoginseng plantations and other land covers for various indices

Index	Jeffries-Matusita (J-M)								SDI
	Vegetation	Water	Soil	Desert	Residential	Shadow	Mean	Sum	Sum
Min	1.152	1.221	0.309	0.933	1.199	1.293	1.018	6.107	7.75
Max	1.413	0.326	1.346	1.406	**1.371**	0.869	1.122	6.732	12.98
NDPI	1.413	1.279	1.414	1.064	1.055	1.226	1.242	7.451	12.91
CSI	1.414	1.063	1.399	1.405	1.340	0.406	1.171	7.027	14.515
MBWI	1.414	1.326	1.410	1.411	1.329	0.268	1.193	7.157	15.552
$AWEI_{nsh}$	1.414	1.034	1.401	1.372	0.901	1.098	1.203	7.220	12.788
MNDWI	1.414	1.250	1.414	**1.414**	1.093	1.235	1.303	7.820	18.06
NDVI	1.414	1.306	1.092	1.362	1.053	**1.371**	1.266	7.599	19.21
$AWEI_{sh}$	1.414	1.250	1.413	1.412	1.350	1.081	1.320	7.920	18.267
NDWI	1.414	1.396	1.414	1.371	1.036	1.361	1.332	7.993	22.03
NDRI	1.414	1.151	1.414	1.413	1.300	1.310	1.334	8.002	22.77
SNRI	**1.414**	**1.414**	**1.414**	1.413	1.300	1.310	**1.378**	**8.265**	**25.43**

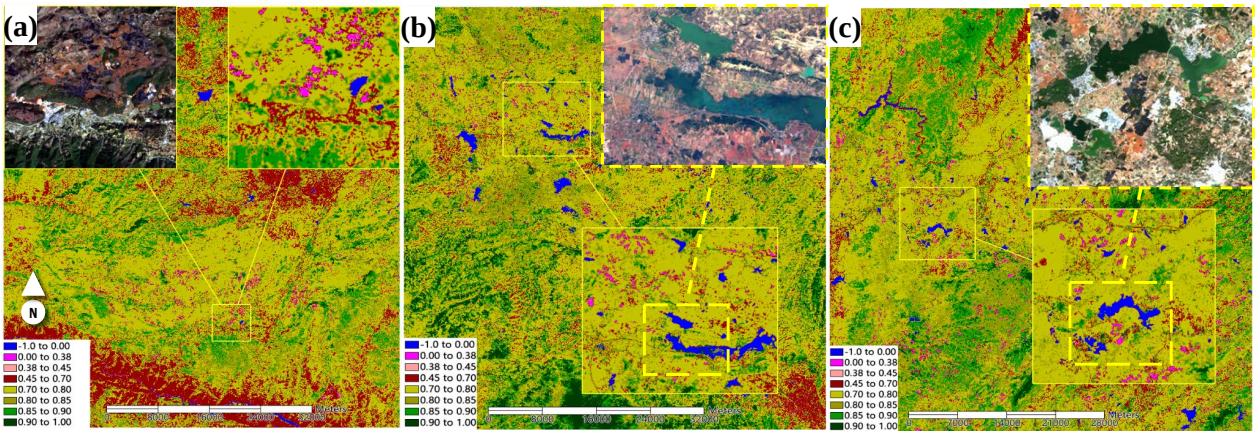

Fig. 3: Raster color slices of SNRI and true color composite images captured by Landsat-8 OLI and Sentinel-2A in the study areas of (a) Honghe, (b) Wenshan, and (c) Qujing.

a maximum J-M of 1.414. For distinguishing sheds from vegetation, SNRI and NDVI had the highest J-M of 1.414. SNRI also had the highest J-M of 1.414, along with NDRI, NDWI, MNDWI, and NDPI, for distinguishing sheds from bare soil. In distinguishing sheds from desert, SNRI had a J-M separability close to MNDWI, reaching 1.413. Most indices performed poorly in separating sheds from residential, with Max performing best (J-M of 1.371), followed by $AWEI_{sh}$. Similarly, the separability of these indices in distinguishing sheds from shadows was unsatisfactory, with NDVI performing best. Overall, SNRI had the highest separability compared to other indices, with SDI and J-M of 25.43 and 8.265, respectively, when considering all background covers versus P. notoginseng sheds.

Since a single index cannot effectively distinguish P. notoginseng plantations from all other land covers, we selected two indices with good separability as input variables for the SVM classifier. Table IV shows the cross-validation accuracy of classification results using different combinations of two indices. The combination of SNRI and Max achieved an F1 value of 0.987 for separating P. notoginseng plantations from other land covers. The overall accuracy was 0.933 with a kappa coefficient of 0.922, indicating successful separation with high precision. In our analysis, we ranked the classification results based on the kappa coefficient in descending order. Notably, among the top four combinations, SNRI was included in three of them. While the SNRI-Max combination's kappa coefficient ranked second after the AWEI-NDVI combination, it demonstrated the highest F1 score and Precision. This finding reinforces the superior performance of SNRI in effectively distinguishing P. notoginseng plantations from other land cover types.

TABLE IV: P. notoginseng plantations extraction accuracy with different two-indies combinations (OA stands for overall accuracy).

	F1	Precision	Recall	OA	kappa
$AWEI_{sh}$-NDVI	0.973	0.962	0.984	**0.937**	**0.925**
SNRI-Max	**0.987**	**0.982**	0.992	0.933	0.922
$AWEI_{sh}$-SNRI	0.974	0.958	0.991	0.927	0.914
SNRI-NDVI	0.917	0.962	0.865	0.912	0.897
NDWI-Max	0.980	0.972	0.993	0.908	0.891
SNRI-MNDWI	0.900	0.877	0.925	0.903	0.886
$AWEI_{nsh}$-NDVI	0.840	0.776	0.918	0.904	0.885
MBWI-NDVI	0.959	0.930	0.991	0.900	0.880
NDVI-Max	0.981	0.966	**0.998**	0.895	0.876
NDVI-MNDWI	0.877	0.843	0.916	0.892	0.873
SNRI-NDWI	0.909	0.877	0.945	0.891	0.872
NDVI-NDWI	0.875	0.834	0.923	0.887	0.867
NDWI-MNDWI	0.875	0.831	0.925	0.817	0.784
MNDWI-Max	0.955	0.922	0.991	0.785	0.747

Authorized licensed use limited to: Xian Jiaotong University. Downloaded on March 20,2024 at 23:26:41 UTC from IEEE Xplore. Restrictions apply.
© 2024 IEEE. Personal use is permitted, but republication/redistribution requires IEEE permission. See https://www.ieee.org/publications/rights/index.html for more information.

This article has been accepted for publication in IEEE Geoscience and Remote Sensing Letters. This is the author's version which has not been fully edited and content may change prior to final publication. Citation information: DOI 10.1109/LGRS.2024.3379196

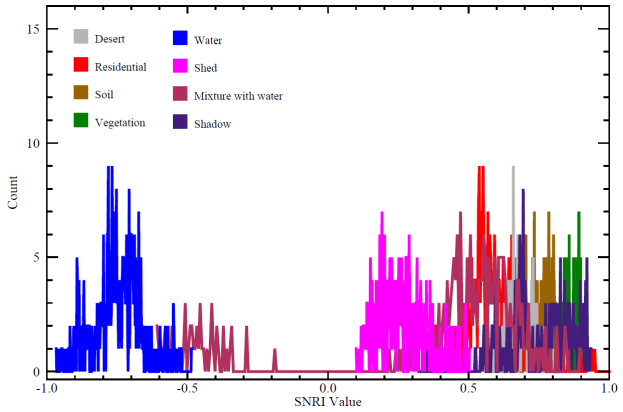

Fig. 4: SNRI statistical histograms of different land covers in the Honghe area.

Despite the effectiveness of SNRI has been tested in the three different study areas, there are still some noteworthy issues to discuss: (1) In the SNRI histograms of land covers, the overlap between water bodies and land, which are located on opposite sides of the sheds (as shown in Fig.4), is commonly observed in the mixed pixels around water bodies; (2) Black sheds' reflectance signal is affected by shading net transmittance. This can cause signal variations from P. notoginseng plantations across different growth stages, altitudes, and climates, potentially impacting SNRI discrimination accuracy; (3) Other agricultural structures, such as certain flower cultivation farms, near urban areas, may also have roofs covered with similar black shading nets, which could potentially lower the extraction accuracy of P. notoginseng plantations. Solving this issue in the spectral feature dimension is challenging because these sheds have the same material. However, by combining the SNRI with the spatio-temporal features of time-series imagery, it becomes possible to help to address these issues.

V. Conclusion

In this study, we have introduced a novel index called the Signed Normalized Range Index (SNRI) for the extraction of P. notoginseng plantations in Yunnan, China, using Landsat-8 OLI images. The development of SNRI is based on a lower reflectance range compared to other land covers, and a negative difference between the Green and NIR bands, which distinguishes them from open water. Both qualitative and quantitative analyses have demonstrated the promising performance of SNRI in enhancing the visibility of P. notoginseng plantations while suppressing noise from other land covers.

Looking ahead, it is promising to explore the application of SNRI in remote sensing estimation and change monitoring of the P. notoginseng planting area, as well as other land covers with similar lower reflectance ranges. This index holds potential for facilitating improved management of P. notoginseng plantations in the region.

References

[1] P. D. Noire and T. Ma, "Microchemical investigation of medicinal plants. xii," *Microchimica Acta*, vol. 64, no. 4, pp. 455–461, 1975.
[2] T. Chou, "The saponins of the chinese drug, san-ch'i, aralia bipinnatifida," *Chin J Physiol*, vol. 12, no. 1, pp. 59–66, 1937.
[3] J. T. Coon and E. Ernst, "Panax ginseng," *Drug safety*, vol. 25, no. 5, pp. 323–344, 2002.
[4] X. M. Cui, L. Q. Huang, L. P. Guo, and D. H. Liu, "Chinese sanqi industry status and development countermeasures," *China Journal of Chinese Materia Medica*, vol. 39, no. 4, pp. 553–557, 2014.
[5] S. Y. Hu, "The genus panax (ginseng) in chinese medicine," *Economic Botany*, vol. 30, no. 1, pp. 11–28, 1976.
[6] C. X. Dai, X. J. Xie, Z. G. Xu, and P. Du, "Monitoring and analyzing herbal medicine plantation via remote sensing: A case study of pseudo-ginseng in wenshan and honghe prefecture of yunnan province," *Remote Sensing for Land and Resources*, vol. 30, no. 1, pp. 210–216, 2018.
[7] Q. Luo, C. M. You, and H. Guan, "Analysis of influences of environmental factors on the growth of panax notoginseng," *Science and Technology of West China*, vol. 9, no. 09, pp. 7–8+12, 2010.
[8] Z. Yang, J. Dong, W. Kou, Y. Qin, and X. Xiao, "Mapping panax notoginseng plantations by using an integrated pixel-and object-based (ipob) approach and zy-3 imagery," *Remote Sensing*, vol. 13, no. 11, p. 2184, 2021.
[9] F. Deng and S. Pu, "Single-class data descriptors for mapping panax notoginseng through p-learning," *Applied Sciences*, vol. 8, no. 9, p. 1448, 2018.
[10] Z. Li, K. Zhang, F. Zhao, and J. Zhang, "Remote sensing monitoring of planting area of panax notoginseng: A case study of kaiyuan city in honghe prefecture," *Journal of Applied Remote Sensing*, vol. 17, no. 1, pp. 018 501–018 501, 2023.
[11] J. Rouse Jr, R. Haas, J. Schell, and D. Deering, "Monitoring vegetation systems in the great plains with erts," in *Third Earth Resources Technology Satellite-1 Symposium: The Proceedings of a Symposium Held by Goddard Space Flight Center at Washington, DC on*, vol. 351, 1973, p. 309.
[12] B.-C. Gao, "Ndwi—a normalized difference water index for remote sensing of vegetation liquid water from space," *Remote sensing of environment*, vol. 58, no. 3, pp. 257–266, 1996.
[13] H. Xu, "Modification of normalised difference water index (ndwi) to enhance open water features in remotely sensed imagery," *International journal of remote sensing*, vol. 27, no. 14, pp. 3025–3033, 2006.
[14] G. L. Feyisa, H. Meilby, R. Fensholt, and S. R. Proud, "Automated water extraction index: A new technique for surface water mapping using landsat imagery," *Remote sensing of environment*, vol. 140, pp. 23–35, 2014.
[15] X. Wang, S. Xie, X. Zhang, C. Chen, H. Guo, J. Du, and Z. Duan, "A robust multi-band water index (mbwi) for automated extraction of surface water from landsat 8 oli imagery," *International Journal of Applied Earth Observation and Geoinformation*, vol. 68, pp. 73–91, 2018.
[16] H. Zhai, H. Zhang, L. Zhang, and P. Li, "Cloud/shadow detection based on spectral indices for multi/hyperspectral optical remote sensing imagery," *ISPRS journal of photogrammetry and remote sensing*, vol. 144, pp. 235–253, 2018.
[17] M. A. Wulder, T. R. Loveland, D. P. Roy, C. J. Crawford, J. G. Masek, C. E. Woodcock, R. G. Allen, M. C. Anderson, A. S. Belward, W. B. Cohen *et al.*, "Current status of landsat program, science, and applications," *Remote sensing of environment*, vol. 225, pp. 127–147, 2019.
[18] J. M. Pereira, "A comparative evaluation of noaa/avhrr vegetation indexes for burned surface detection and mapping," *IEEE transactions on geoscience and remote sensing*, vol. 37, no. 1, pp. 217–226, 1999.
[19] R. Sonobe, Y. Yamaya, H. Tani, X. Wang, N. Kobayashi, and K.-i. Mochizuki, "Assessing the suitability of data from sentinel-1a and 2a for crop classification," *GIScience & Remote Sensing*, vol. 54, no. 6, pp. 918–938, 2017.
[20] S. Gunal and R. Edizkan, "Subspace based feature selection for pattern recognition," *Information Sciences*, vol. 178, no. 19, pp. 3716–3726, 2008.

Authorized licensed use limited to: Xian Jiaotong University. Downloaded on March 20,2024 at 23:26:41 UTC from IEEE Xplore. Restrictions apply.
© 2024 IEEE. Personal use is permitted, but republication/redistribution requires IEEE permission. See https://www.ieee.org/publications/rights/index.html for more information.